

Flat band and η -pairing states in one-dimensional Moiré Hubbard model

R. Wang, and Z. Song*

School of Physics, Nankai University, Tianjin 300071, China

A moiré system is formed when two periodic structures have a slightly mismatched period, resulting in unusual strongly correlated states in the presence of particle-particle interactions. The periodic structures can arise from the intrinsic crystalline order and periodic external field. We investigate a one-dimensional Hubbard models with periodic on-site potential of period n_0 , which is commensurate to the lattice constant. For large n_0 , exact solution demonstrates that there is a midgap flat band with zero energy in the absence of Hubbard interaction. Each moiré unit cell contributes two zero energy levels to the flat band. In the presence of Hubbard interaction, the midgap physics is demonstrated to be well described by a uniform Hubbard chain, in which the effective hopping and on-site interaction strength, can be controlled by the amplitude and period of the external field. Numerical simulations are performed to demonstrate the correlated behaviors in the finite-sized moiré Hubbard system, including the existence of η -pairing state, and bound pair oscillation. This finding provides a method to enhance the correlated effect by a spatially periodic external field.

I. INTRODUCTION

The theoretical and experimental studies on twisted bilayer graphene (TBG) indicate that the interplay of lattice geometry and many-body interactions can induce exotic quantum states [1–7], which include superconducting and correlated insulating behavior. In general, these phenomena are known to arise from the formation of flat band with low energy and narrow bandwidth, which greatly enhances the electronic interaction effect. However, it is a little tough to observe these interesting correlation-induced phenomena because accurate magic angle in TBG brings constraints on device fabrication. Therefore, it is natural to look for a one-dimensional version of TBG, providing easier access to the flat band by alternative approaches. A starting point is the moiré patterns, which emerge due to the superposition of two periodic structures, with either slightly different periods or different orientations, such patterns have been realized in materials [8–14].

In principle, a one-dimensional moiré system can be deliberately engineered as a super-long-period system when the periods of two ingredients are slightly different but commensurate [15–17]. It is essentially a one-dimensional periodic system with a large unit cell, which may result in weak inter-unit-cell coupling, or nearly flat band. Theoretically, two periodic structures can arise from the intrinsic crystalline order and periodic external field. In condensed matter, particles are usually confined by a periodic potential in synthetic and natural materials. Another periodic structure can come from another external field. Comparing to magic angle in TBG, the amplitude and period of a periodic external field may be easy to control in experiment.

In this paper, we investigate a moiré Hubbard model, which is a uniform Hubbard chain subjected to a field

by sinusoidal modulation with period commensurate to the lattice constant. In the absence of the Hubbard interaction, a midgap flat band is induced by the periodic field when the field amplitude or the superlattice unit cell is large enough. We determine that the corresponding eigen wave functions are Gaussian-like with their centers located at each zero potential point. When the field strength or unit cell decreases, the flat band become narrow band, which can be well characterized by tight-binding approximation, the Gaussian-like wave functions playing the role of Wannier functions. In the presence of the Hubbard interaction, the moiré pattern physics is demonstrated to be well described by a uniform Hubbard chain with effective hopping (J_{eff}) and on-site interaction strength (U_{eff}). Importantly, the ratio $U_{\text{eff}}/J_{\text{eff}}$ can be controlled by the amplitude and period of the external field, to achieve the goal of enhancing the electronic interaction effect. Numerical simulations are performed to demonstrate the correlated behaviors of an ordinary Hubbard model in the finite-sized moiré Hubbard system. The first one is the existence of η -pairing state, which is believed as a possible mechanism of superconductivity based on the concept off-diagonal long-range order (ODLRO). Another is the bound pair oscillation, demonstrating a correlated dynamics. This finding provides a theoretical model as one-dimensional analogue of twisted bilayer graphene. The advantage of this method is that the correlated effect can be enhanced by the external field. We expect our results benefit to experimental research.

This paper is organized as follows. In Section II, we present a one-dimensional Hubbard model with a spatially modulated on-site potential. In Section III, we discuss midgap physics in the model. In Section IV, we propose a dynamic scheme to experimentally demonstrate that the moiré Hubbard model supports midgap bound-pair states. Finally, we provide a summary in Section V.

* songtc@nankai.edu.cn

II. MODEL HAMILTONIAN

We consider a one-dimensional Hubbard model with a spatially modulated on-site potential

$$H = H_0 + U \sum_j n_{j,\uparrow} n_{j,\downarrow} \quad (1)$$

with

$$H_0 = \sum_{j,\sigma=\uparrow,\downarrow} [-\kappa c_{j,\sigma}^\dagger c_{j+1,\sigma} + \text{H.c.} + (-1)^j V \times \cos(\frac{\pi j}{n_0}) n_{j,\sigma}], \quad (2)$$

where $c_{j,\sigma}$ ($c_{j,\sigma}^\dagger$) is the annihilation (creation) operator for an electron at site j with spin σ and $n_{j,\sigma} = c_{j,\sigma}^\dagger c_{j,\sigma}$. We schematically illustrate that such a potential can be realized by a continuous potential of trigonometric function (see Fig. 1). H is known as a one-dimensional standard Hubbard model with the uniform case ($V = 0$), which has been studied in many perspectives [18, 19]. However, this work investigates on the effect of nonzero V on the property of Hubbard model. Parameters κ and U play the role of kinetic and interaction energy scale, respectively. The on-site staggered potential is commensurate for integer n_0 , which determines the Morie period $2n_0$. We consider a ring lattice of length $N = 2Mn_0$ and take $c_{N+1,\sigma} \equiv c_{1,\sigma}$ to impose a periodic boundary condition. The main results of this work are independent of the boundary conditions.

We focus on the interaction-free case with zero U and rewrite H_0 as the form of

$$H_0 = \sum_{m=1}^M \left[\sum_{l=1}^{2n_0-1} (-\kappa) (c_{m,l}^\dagger c_{m,l+1} + c_{m,2n_0}^\dagger c_{m+1,1} + \text{H.c.}) + \sum_{l=1}^{2n_0} (-1)^l V \cos(\frac{\pi l}{n_0}) n_{m,l} \right], \quad (3)$$

where we neglect the index of σ , with the mapping $c_{2(m-1)n_0+l,\sigma} = c_{m,l}$ and $n_{m,l} = c_{m,l}^\dagger c_{m,l}$. Here index m denotes the unit cell, while l denotes the position of the site in the m -th unit cell. We impose the periodic boundary condition $c_{M+1,1} = c_{1,1}$ and perform the Fourier transformations

$$c_{m,l} = \frac{1}{\sqrt{M}} \sum_k e^{ikm} c_{k,l}, \quad (4)$$

with $k = 2n\pi/M$, $n = 0, 1, \dots, M-1$. Therefore, the transformation block diagonalizes the Hamiltonian with translational symmetry, that is, H_0 can be written as block-diagonal form of

$$H_0 = \sum_k H_{0k} = \sum_k \psi_k^\dagger h_{0k} \psi_k, \quad (5)$$

satisfying $[H_{0k}, H_{0k'}] = 0$, in which the operator vector is

$$\psi_k = (c_{k,1}, c_{k,2}, \dots, c_{k,2n_0})^T, \quad (6)$$

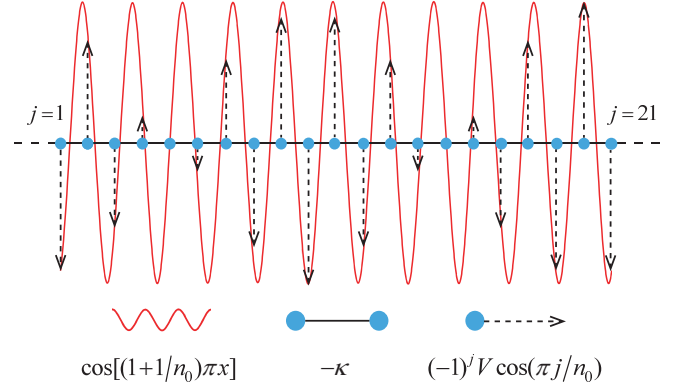


FIG. 1. Schematic illustration of a one-dimensional moiré system, which consists two periodic ingredients with different but commensurate periods. The lattice (array of solid blue circles) constant is 1, while the external field (red line) is cosinusoidal function $\cos[(1+1/n_0)\pi x]$ with period $2/(1+1/n_0)$. The whole system is still periodic with a long period $2n_0$ for large n_0 . The dotted arrow denotes the on-site potential distribution on the lattice, which is spatially modulated and staggered as $(-1)^j \cos(\pi j/n_0)$ in Eq. (2), where $j = \text{INT}(x)$ is integer portion of the coordinate x . Here $-\kappa$ is nearest-neighbour hopping strength and $n_0 = 10$.

and h_{0k} is a $2n_0 \times 2n_0$ matrix

$$h_{0k} = \begin{pmatrix} A_1 & -\kappa & 0 & \cdots & & -\kappa e^{-ik} \\ -\kappa & A_2 & -\kappa & 0 & \cdots & \\ 0 & -\kappa & A_3 & -\kappa & 0 & \cdots \\ \vdots & 0 & -\kappa & \ddots & & \\ & \vdots & 0 & & & \\ & & \vdots & & \ddots & -\kappa \\ -\kappa e^{ik} & & & & -\kappa & A_{2n_0} \end{pmatrix} \quad (7)$$

with $A_l = (-1)^l V \cos(\pi l/n_0)$. Matrix h_{0k} corresponds to a uniformly hopping ring with non-uniform on-site potential and a threading flux k through it. The flux can be neglected in large n_0 limit. The system then has approximate reflection symmetry about the site n_0 due to the fact $A_{2n_0-l} = A_l$. The eigenvector of h_{0k} has the form of

$$\varphi_0(k, n) = \sum_l^{2n_0} f_{k,l}^n c_{k,l}^\dagger, \quad (8)$$

where $n = 1, 2, \dots, 2n_0$, denotes the energy level index $E_{0k}(n)$. Exact solution of $\{f_{k,l}^n\}$ is tough to be obtained. However, there are M pairs of zero potential points at $(m, l) = (m, n_0/2)$ and $(m, 3n_0/2)$ (or $j = 2n_0(m-1) + n_0/2$ and $2n_0(m-1) + 3n_0/2$ for the original coordinate) in the limit case with $n_0 \gg 1$ and nonzero V . In the following, we will demonstrate that there are M pairs of zero energy eigenvectors.

As an approximation, we take a linearization of the Hamiltonian as effective Hamiltonian by Taylor expan-

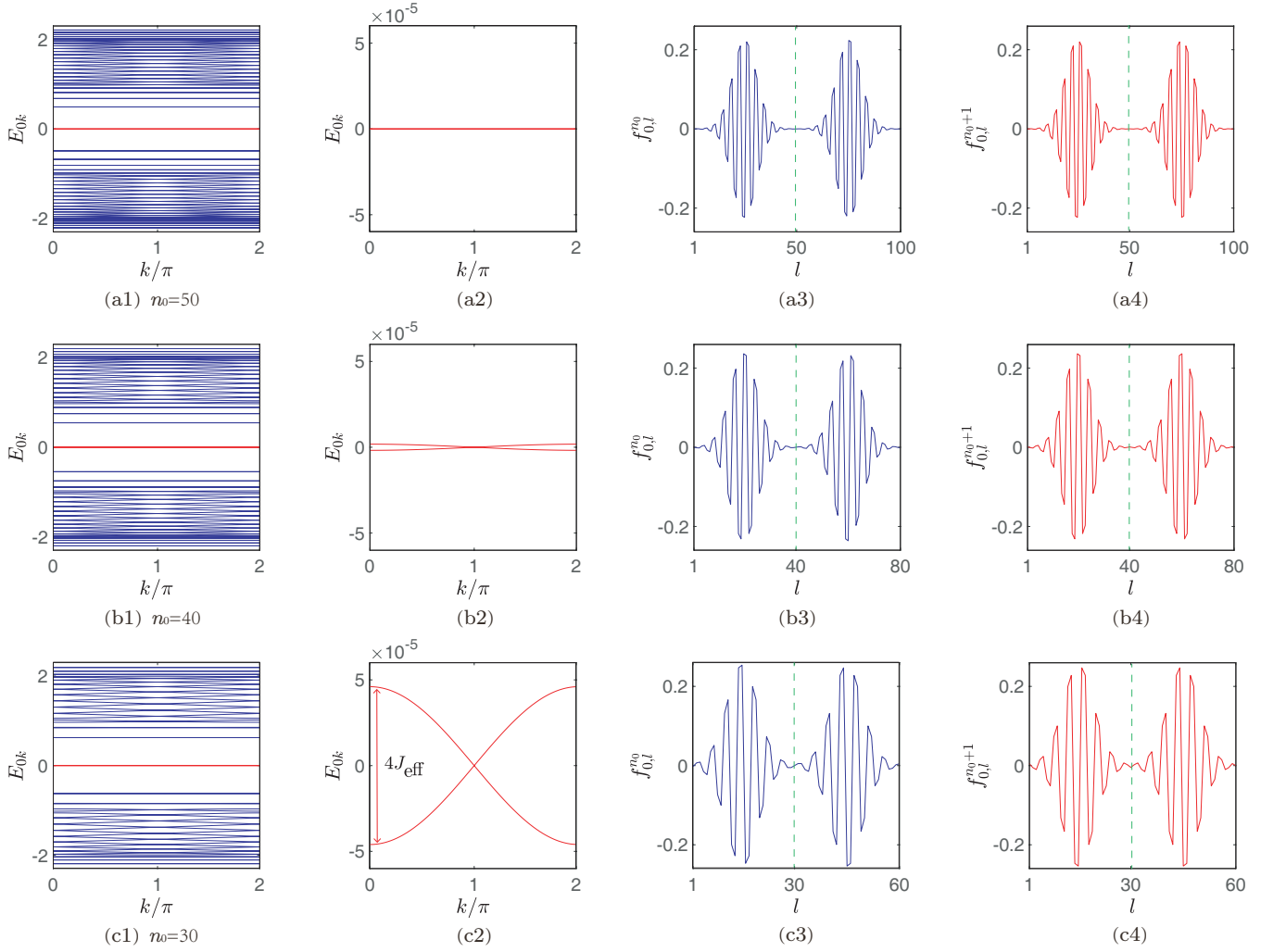


FIG. 2. Plots of energy spectra (a1-c1) and selected midgap wave functions (a3-c3) and (a4-c4), obtained from exact diagonalization of the matrix in Eq. (7) for fixed V and three typical $n_0 = 50, 40,$ and 30 , respectively. (a2-c2) is zoom of (a1-c1), selected typical energy levels around zero energy. We only plot the wave functions in a single unit cell with $k = 0$. We determine that the zero energy states are antisymmetric (blue) and symmetric (red) about the point $l = n_0$ (green dotted line), which accords to the fact that H_0^{eff} in Eq. (9) has reflection symmetry. As n_0 decreases, the width of the wavepackets increases and the overlap between two neighbour ones appears. Meanwhile, the midgap flat band becomes midgap narrow band. The energy unit is κ . The system parameters are $\kappa = V = 1$, and $M = 100$.

sion of the potential around each zero potential points. Defining Λ as the range of validity for this linearization approximation, we write the linearized effective Hamiltonian as the form of

$$H_0^{\text{eff}} = \sum_k (H_{0k}^+ + H_{0k}^-), \quad (9)$$

where

$$H_{0k}^{\pm} = \sum_{l=n_0 \pm n_0/2 - \Lambda}^{n_0 \pm n_0/2 + \Lambda} [-\kappa c_{k,l}^{\dagger} c_{k,l+1} + \text{H.c.} \mp (-1)^l V \times (n_0 \pm n_0/2 - \frac{\pi l}{n_0}) n_{k,l}]. \quad (10)$$

We determine that H_0^{eff} has reflection symmetry about

the point $l = n_0$, as mentioned of the approximate symmetry of h_{0k} . Introducing a set of operators defined by

$$\phi_{\pm}^{\dagger}(k) = \left(\frac{V}{2\kappa n_0}\right)^{1/4} \sum_{l=n_0 \pm n_0/2 - \Lambda}^{n_0 \pm n_0/2 + \Lambda} \sin[(1+2l)\pi/4] \times e^{-\frac{V\pi}{4\kappa n_0}[l-(n_0 \pm n_0/2)]^2} c_{k,l}^{\dagger}, \quad (11)$$

a straightforward derivation demonstrates

$$[H_0^{\text{eff}}, \phi_{\pm}^{\dagger}(k)] \approx 0. \quad (12)$$

It approximately indicates that a set of states $\phi_{\pm}^{\dagger}(k)|0\rangle$ are eigenstates of H_0^{eff} with zero energy. Similarly, a set

of local Gaussian wavepackets $\phi_{\pm}^{\dagger}(m)|0\rangle$ with

$$\begin{aligned} \phi_{\pm}^{\dagger}(m) &= \left(\frac{V}{2\kappa n_0}\right)^{1/4} \sum_{l=n_0 \pm n_0/2 - \Lambda}^{n_0 \pm n_0/2 + \Lambda} \sin[(1+2l)\pi/4] \\ &\times e^{-\frac{V\pi}{4\kappa n_0}[l-(n_0 \pm n_0/2)]^2} e^{ikm} c_{m,l}^{\dagger} \end{aligned} \quad (13)$$

are eigenstates of H_0^{eff} with zero energy, where $|0\rangle$ is the vacuum state for the creation fermion operator $c_{m,l}^{\dagger}$. It is easy to check that there are totally $2M$ zero energy eigenvectors.

Eigenvector $\varphi_0(k, n)$ and spectrum $E_{0k}(n)$ can be obtained numerically by exact diagonalization of the matrix h_{0k} in the case of finite n_0 limit. We plot the profiles of the wave function and the spectrum for three representative cases (see Fig. 2). We determine that for sufficient large n_0 , the zero energy states are separated Gaussian wavepackets, which accords to our above analysis. As n_0 decreases, the width of the wavepackets increases and the overlap between two neighbour ones appears. Moreover, the midgap flat band becomes midgap narrow band. Similar things happen as fix n_0 and vary V : there is a midgap flat band in large V limit with $V \gg \kappa$ because every zero potential sites decouple from the neighbours. Extreme localized states (site state) form at each zero potential points. As V decreases, the site state becomes wavepacket and as its width increases, the overlap between two neighbour ones appears. Each zero potential points become the centers of wavepackets. Moreover, the midgap flat band becomes midgap narrow band. This process is demonstrated by numerical simulation in Fig. 3.

It is clear that this moiré system can be regarded as a superlattice: $\phi_{\pm}(m)$ [$\phi_{\pm}^{\dagger}(m)$] annihilates (creates) a localized Wannier state at superlattice site m . The midgap band is depicted by tight-binding Hamiltonian

$$\begin{aligned} H_0^{\text{MG}} &= J_{\text{eff}} \sum_m [\phi_{+}^{\dagger}(m)\phi_{-}(m) \\ &+ \phi_{+}^{\dagger}(m)\phi_{-}(m+1) + \text{H.c.}]. \end{aligned} \quad (14)$$

The hopping constant J_{eff} can be estimated from numerical result for the width ($4J_{\text{eff}}$) of midgap narrow band as indicated in Fig. 2(c2). We would like to point out that, unlike the usual single lowest band approximation, J_{eff} is always positive, since H_0^{MG} describes a midgap band, does not violate the node theorem for the eigen wave function in one-dimensional system.

III. MIDGAP HUBBARD MODEL

So far we have established the tight binding description of the midgap physics for the moiré system. In the following section, we will consider the case with nonzero U . H_0^{MG} then can be modified by adding the spin index, replacing $\phi_{\pm}(m)$ by $\phi_{\pm,\sigma}(m)$. The above analysis

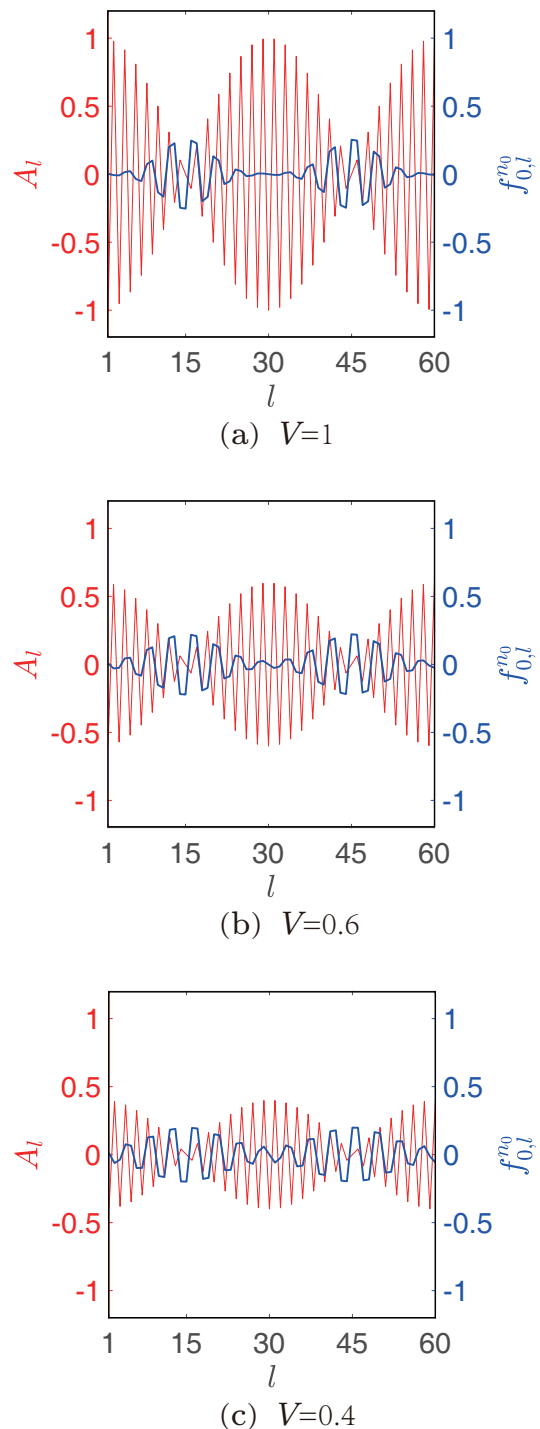


FIG. 3. Plots of the profiles of wave functions (blue) in the midgap and on-site potential distribution A_l (red). Three representative values of V are selected and the corresponding wave functions $f_{k,l}^n$ with $k=0$ are obtained by exact diagonalization of matrix in Eq. (7). As expected, we see that the wave functions are Gaussian-like with the center being localized around zero potential points. The width of wavepackets increases and the overlap between two neighbour ones appears as V decreases. The system parameters are $\kappa=1$, and $n_0=30$.

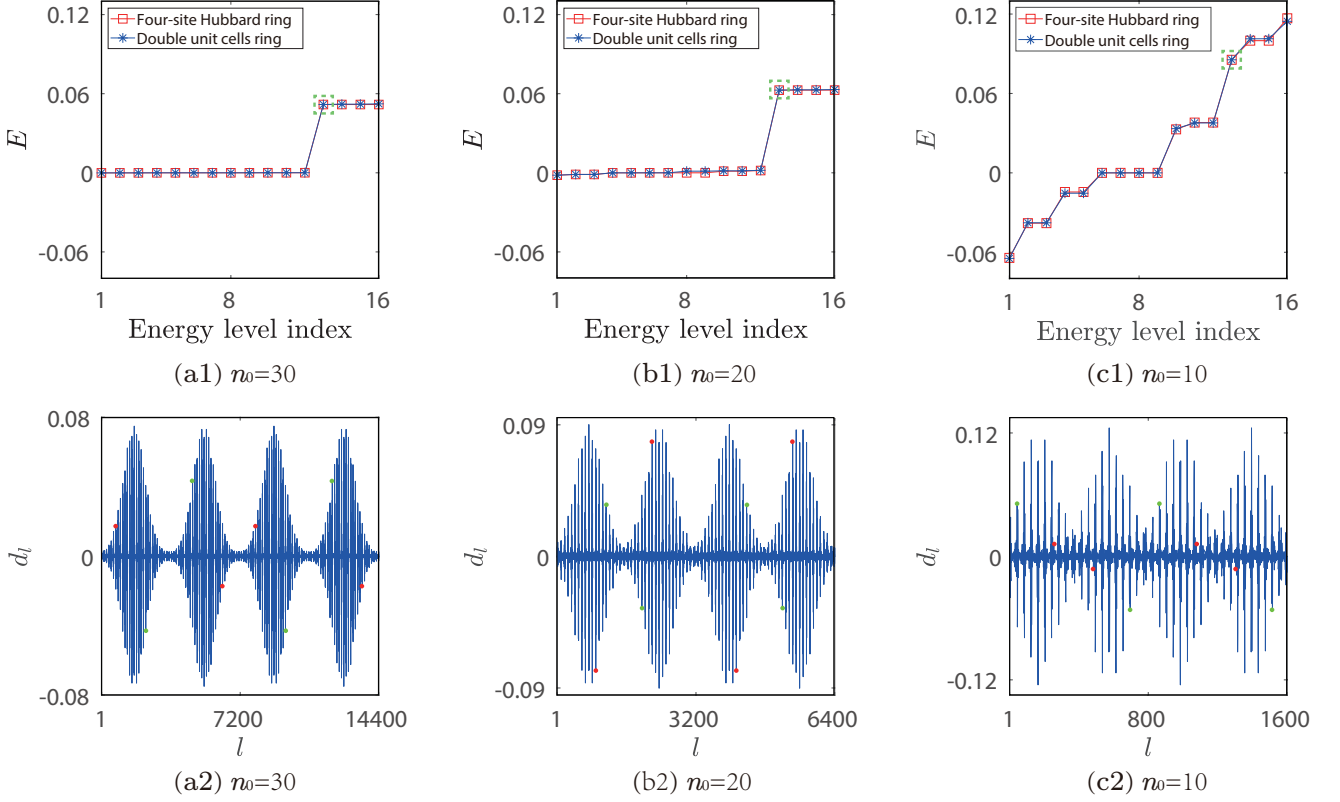


FIG. 4. Comparison of the midgap states of moiré Hubbard model and its tight-binding description. (a1-c1) Plots of midgap energy levels (blue star) obtained by exact diagonalization of the Hamiltonian in Eq. (18) for three typical n_0 . Red squares stand for the energy levels of a four-site Hubbard ring with fitting values of J_{eff} and U_{eff} . We can find that for sufficient large n_0 , the original single flat band ($U = 0$) separates into two flat bands (a1), the upper band is pair band. As n_0 decreases, the width of the two bands increase [(b1) and (c1)]. The pair-band is fitted by the numerical result from the four-site Hubbard ring in Eq. (15). The fitting parameters of four-site Hubbard ring are $J_{\text{eff}} = 2.30 \times 10^{-5}$, $U_{\text{eff}} = 5.18 \times 10^{-2}$ (5.11×10^{-2}) in (a1), $J_{\text{eff}} = 6.20 \times 10^{-4}$, $U_{\text{eff}} = 6.27 \times 10^{-2}$ (6.14×10^{-2}) in (b1), and $J_{\text{eff}} = 1.90 \times 10^{-2}$, $U_{\text{eff}} = 8.54 \times 10^{-2}$ (8.42×10^{-2}) in (c1), respectively. Here the values of U_{eff} in each bracket are obtained from Eq. (17). (a2-c2) Plots of the eigen wave function d_l of the lowest energy level, i.e., $E = U_{\text{eff}}$ (green dashed box) at the upper band. It is the η -pairing state, which obeys the relation in Eq. (28) as expected, indicating by two groups of red and green solid circles. The results demonstrate that the tight-binding approximation works quite well and there exist η -pairing states in the superlattice near the Fermi level. The system parameters are $\kappa = 1$, $V = 1$, and $U = 0.5$.

still holds for interaction-free terms ($H_{0,\sigma}^{\text{MG}}$). The midgap Hubbard model Hamiltonian reads

$$H^{\text{MG}} = \sum_{\sigma=\uparrow,\downarrow} H_{0,\sigma}^{\text{MG}} + U_{\text{eff}} \sum_{m,\rho=\pm} \phi_{\rho,\uparrow}^\dagger(m) \phi_{\rho,\uparrow}(m) \times \phi_{\rho,\downarrow}^\dagger(m) \phi_{\rho,\downarrow}(m), \quad (15)$$

where $H_{0,\sigma}^{\text{MG}}$ is extended from H_0^{MG} , which has the form of

$$H_{0,\sigma}^{\text{MG}} = J_{\text{eff}} \sum_m [\phi_{+,\sigma}^\dagger(m) \phi_{-,\sigma}(m) + \phi_{+,\sigma}^\dagger(m) \phi_{-,\sigma}(m+1) + \text{H.c.}], \quad (16)$$

The effective Hubbard interaction strength U_{eff} is determined by

$$U_{\text{eff}} = U \langle 0 | \phi_{\rho,\downarrow}(m) \phi_{\rho,\uparrow}(m) [\sum_l (n_{m,l,\uparrow} n_{m,l,\downarrow})] \times \phi_{\rho,\uparrow}^\dagger(m) \phi_{\rho,\downarrow}^\dagger(m) | 0 \rangle, \quad (17)$$

which can be estimated by numerical computation. We plot the profiles of the two-particle eigenstates and the spectrum for three representative cases (see Fig. 4). We determine that for sufficient large n_0 , the flat band separates into two flat bands, one is pair-band, another is scattering band. The width of the two bands increases as n_0 decreases.

To verify the tight-binding approximation, one can fit the result from exact diagonalization for original Hamiltonian by that of H^{MG} . We consider a system with

double moiré unit cells,

$$H_{M2} = \sum_{j=1, \sigma=\uparrow, \downarrow}^{4n_0} [-\kappa c_{j, \sigma}^\dagger c_{j+1, \sigma} + \text{H.c.} + (-1)^j V] \\ \times \cos\left(\frac{\pi j}{n_0}\right) n_{j, \sigma} + U \sum_{j=1}^{4n_0} n_{j, \uparrow} n_{j, \downarrow}, \quad (18)$$

which corresponds to a four-site Hubbard ring.

Besides the Eq. (17), U_{eff} can further be obtained by fitting the energy levels of H_{M2} to that of H^{MG} . The fitting results are given in Fig. 4(a1-c1), and the obtained U_{eff} by fitting is compared with the value estimated from Eq. (17). We determine that the approximation works quite well. Furthermore, the bound-pair levels [upper band in Fig. 4(a1-c1)] accords with the analytical expression

$$\varepsilon_n = \sqrt{U_{\text{eff}}^2 + 16J_{\text{eff}}^2 \cos^2\left(\frac{n\pi}{M}\right)}, \quad (19)$$

with $n = 0, 1, \dots, 2M - 1$, which is obtained in the previous works [20, 21].

Particularly, when taking $n = M/2$, we have $\varepsilon_{M/2} = U_{\text{eff}}$, which is the lowest bound-pair energy level. The corresponding eigenstate is

$$|\Psi_\eta^1\rangle = \eta |0\rangle, \quad (20)$$

where η is the so-called η -pairing operator defined as

$$\eta = \frac{1}{\sqrt{2M}} \sum_{m=1, \rho=\pm}^M \rho \phi_{\rho, \uparrow}^\dagger(m) \phi_{\rho, \downarrow}^\dagger(m). \quad (21)$$

According to the seminal work by Yang [22], we have

$$[H^{\text{MG}}, \eta] = U_{\text{eff}} \eta, \quad (22)$$

which ensures that

$$H^{\text{MG}} |\Psi_\eta^n\rangle = n U_{\text{eff}} |\Psi_\eta^n\rangle, \quad (23)$$

i.e., state

$$|\Psi_\eta^n\rangle = \eta^n |0\rangle, \quad (24)$$

is the eigenstates of H^{MG} with energy nU_{eff} . The η -pairing state $|\Psi_\eta^n\rangle$ has been demonstrated to have ODLRO if n/M is finite ($0 < n/M < 1$) in the thermodynamic limit, $M \rightarrow \infty$.

In general, a complete set basis of the two-electron subspace $\{|l\rangle\}$ is

$$|l\rangle = c_{i, \uparrow}^\dagger c_{j, \downarrow}^\dagger |0\rangle, \quad (25)$$

where l is defined as $l = 2Mn_0(i - 1) + j$, with $i, j \in [1, 2Mn_0]$. Any two-electron states with opposite spins then can be expressed in the form of

$$|\Psi\rangle = \sum_l d_l |l\rangle. \quad (26)$$

For small size moiré Hubbard model H_{M2} with a pair of electrons, the corresponding η -pairing state is

$$|\Psi_\eta^1\rangle = \frac{1}{2} \sum_{\rho=\pm} \rho [\phi_{\rho, \uparrow}^\dagger(1) \phi_{\rho, \downarrow}^\dagger(1) + \phi_{\rho, \uparrow}^\dagger(2) \phi_{\rho, \downarrow}^\dagger(2)] |0\rangle, \quad (27)$$

which requires the eigen wave function with energy U_{eff} satisfies the relation

$$d_l = -d_{4(Mn_0)^2 - l}, \quad l \in [1, 2(Mn_0)^2]. \quad (28)$$

Numerical results for eigen wave function plotted in Fig. 4(a2)-(c2) accord with this analysis. These findings demonstrate that midgap physics for the Hubbard moiré system can be well captured by a simple Hubbard model. The advantage of this system are evident: the parameters J_{eff} and U_{eff} can be controlled by the external field, similar to what happens in optical lattice system. Moreover, midgap Hubbard model provides a possibility to realize one-dimensional superconducting state based on the formation of η pairs near the Fermi level.

IV. BOUND-PAIR DYNAMICS

The above analysis indicates that the moiré Hubbard model supports midgap bound-pair states, which are protected from thermal fluctuation due to energy gap. This may be allowed to observe the related dynamics in experiment, similar to the Bloch oscillation [23]. To verify and demonstrate such a prediction, we consider a simplest case which is consisted of a single moiré unit cell and investigate the dynamics of the system with specific parameters.

The corresponding tight-binding Hamiltonian reads

$$H_1^{\text{MG}} = J_{\text{eff}} [\phi_+^\dagger(1) \phi_-(1) + \text{H.c.}] + U_{\text{eff}} \\ \times \sum_{\rho=\pm} \phi_{\rho, \uparrow}^\dagger(1) \phi_{\rho, \uparrow}(1) \phi_{\rho, \downarrow}^\dagger(1) \phi_{\rho, \downarrow}(1), \quad (29)$$

which is a two-site Hubbard model. In the two-particle invariant subspace, spanned by two-particle basis

$$\left\{ \begin{array}{l} \phi_{+, \uparrow}^\dagger(1) \phi_{+, \downarrow}^\dagger(1) |0\rangle \\ \phi_{-, \uparrow}^\dagger(1) \phi_{-, \downarrow}^\dagger(1) |0\rangle \\ \phi_{+, \uparrow}^\dagger(1) \phi_{-, \downarrow}^\dagger(1) |0\rangle \\ \phi_{-, \uparrow}^\dagger(1) \phi_{+, \downarrow}^\dagger(1) |0\rangle \end{array} \right\}, \quad (30)$$

the matrix representation of H_1^{MG} is

$$h_1 = J_{\text{eff}} \begin{pmatrix} U_{\text{eff}}/J_{\text{eff}} & 0 & 1 & 1 \\ 0 & U_{\text{eff}}/J_{\text{eff}} & 1 & 1 \\ 1 & 1 & 0 & 0 \\ 1 & 1 & 0 & 0 \end{pmatrix}, \quad (31)$$

which has parity symmetry, i.e., $Ph_1P^{-1} = h_1$. The reflectional operator P is defined as $P\phi_{\rho, \sigma}^\dagger(1)P^{-1} = \phi_{\rho, \sigma}^\dagger(1)$

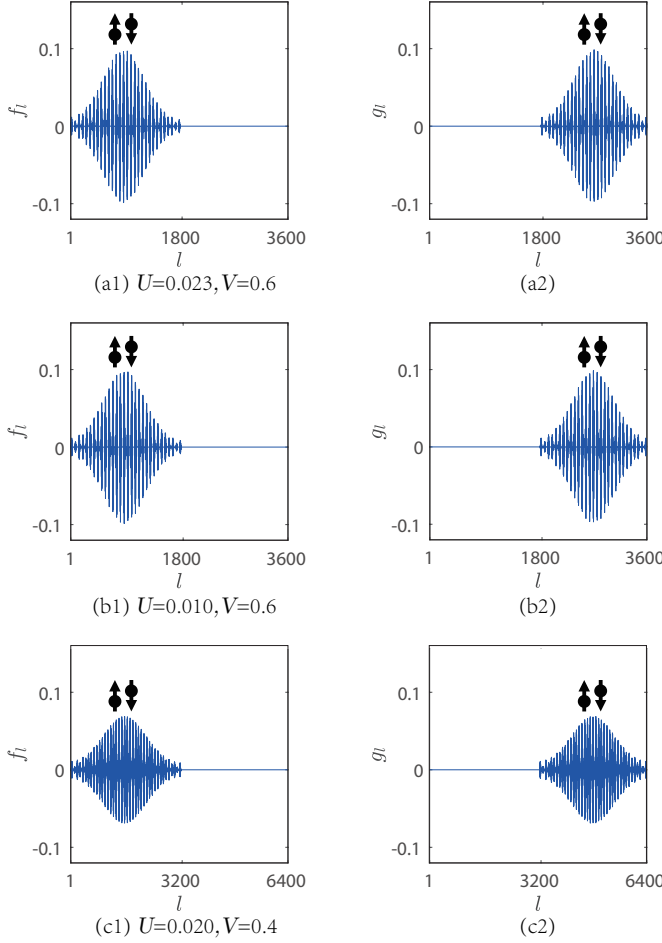


FIG. 5. Profiles of the initial and target states in Eq. (40), the coefficients f_l and g_l with $\kappa = \kappa_0$, obtained by exact diagonalization. Plots of f_l in (a1-c1) and g_l in (a2-c2) for three typical situations. The system parameters are $n_0 = 30$, $U = 0.023$, $V = 0.6$ in (a1-a2), $n_0 = 30$, $U = 0.010$, $V = 0.6$ in (b1-b2), $n_0 = 40$, $U = 0.020$, $V = 0.4$ in (c1-c2), and $\kappa = 1$.

with $\rho = -\bar{\rho} = +, -$ and $\sigma = \uparrow, \downarrow$. Its matrix representation is

$$P = \begin{pmatrix} 0 & 1 & 0 & 0 \\ 1 & 0 & 0 & 0 \\ 0 & 0 & 0 & 1 \\ 0 & 0 & 1 & 0 \end{pmatrix}, \quad (32)$$

in the basis set of Eq. (30). Therefore, four eigenvectors have even or odd parity, i.e.,

$$\begin{cases} P|\psi_1\rangle = |\psi_1\rangle \\ P|\psi_2\rangle = -|\psi_2\rangle \\ P|\psi_3\rangle = -|\psi_3\rangle \\ P|\psi_4\rangle = |\psi_4\rangle \end{cases}, \quad (33)$$

where the eigenvalues and eigenvectors are

$$\varepsilon_2 = U_{\text{eff}}, \varepsilon_3 = 0, \quad (34)$$

$$\varepsilon_{1,4} = \frac{1}{2}(U_{\text{eff}} \pm \sqrt{U_{\text{eff}}^2 + 16J_{\text{eff}}^2}),$$

and

$$\begin{aligned} |\psi_2\rangle &= 2^{-1/2}(-1 \ 1 \ 0 \ 0)^T, \\ |\psi_3\rangle &= 2^{-1/2}(0 \ 0 \ -1 \ 1)^T, \\ |\psi_{1,4}\rangle &= (8 + 2|\varepsilon_{4,1}|^2)^{-1/2}(-2 \ -2 \ \varepsilon_{4,1} \ \varepsilon_{4,1})^T, \end{aligned} \quad (35)$$

respectively. This system allows a special dynamics if we take

$$U_{\text{eff}} = 2\Delta/(2n+1) = 4J_{\text{eff}}/\sqrt{(2n+1)(2n+3)}, \quad (36)$$

at which we simply have

$$\varepsilon_1 = \left(\frac{2n+3}{2n+1}\right)\Delta, \varepsilon_2 = \frac{2}{2n+1}\Delta, \varepsilon_3 = 0, \varepsilon_4 = -\Delta, \quad (37)$$

where $n = 0, 1, 2, \dots$. Such a commensurate energy level structure, together with the parities of the eigenvectors, allows the time evolution operator $U(t) = e^{-i\hat{h}_1 t}$ to obey the connection to the parity operator

$$U(t_q) = (-P)^q \quad (38)$$

at instant $t_q = q(2n+1)\pi/\Delta$. An arbitrary initial state can evolve naturally to its parity counterpart or itself periodically. For example, a Hubbard-pair initial state $\phi_{+,\uparrow}^\dagger(1)\phi_{+,\downarrow}^\dagger(1)|0\rangle$ can evolve to another Hubbard-pair state $\phi_{-,\uparrow}^\dagger(1)\phi_{-,\downarrow}^\dagger(1)|0\rangle$, realizing pair tunneling.

We investigate the tight-binding approximation by numerical simulation of the dynamics in the original system with Eq. (1). We consider the Hamiltonian of a single moiré unit cell,

$$\begin{aligned} H_{M1} &= \sum_{j=1, \sigma=\uparrow, \downarrow}^{2n_0} [-\kappa c_{j,\sigma}^\dagger c_{j+1,\sigma} + \text{H.c.} + (-1)^j V \\ &\quad \times \cos\left(\frac{\pi j}{n_0}\right) n_{j,\sigma}] + U \sum_{j=1}^{2n_0} n_{j,\uparrow} n_{j,\downarrow} \\ &\quad + \kappa_0 \sum_{\sigma=\uparrow, \downarrow} (c_{n_0,\sigma}^\dagger c_{n_0+1,\sigma} + \text{H.c.}), \end{aligned} \quad (39)$$

where the κ_0 term controls the connection between to halves of the chain: when taking $\kappa_0 = \kappa$, we have $J_{\text{eff}} = 0$. The computation is performed in two-particle subspace, where two particles have opposite spins. The subspace is spanned by a set of basis $\{c_{i,\uparrow}^\dagger c_{j,\downarrow}^\dagger |0\rangle, i, j = 1, \dots, 2n_0\}$ of $(2n_0)^2$ dimensions.

We compute the initial state $|\psi_I\rangle$ and target state $|\psi_T\rangle$, by exact diagonalization method for the system of Eq. (39) with $\kappa_0 = \kappa$. The initial state $|\psi_I\rangle$ and target state $|\psi_T\rangle$ has the form

$$\begin{aligned} |\psi_I\rangle &= \sum_l f_l c_{i,\uparrow}^\dagger c_{j,\downarrow}^\dagger |0\rangle, \\ |\psi_T\rangle &= \sum_l g_l c_{i,\uparrow}^\dagger c_{j,\downarrow}^\dagger |0\rangle, \end{aligned} \quad (40)$$

where $l = 2n_0(i-1) + j$. Two states $|\psi_I\rangle$ and $|\psi_T\rangle$ are mutual parity counterpart due to the symmetry of H_{M1} .

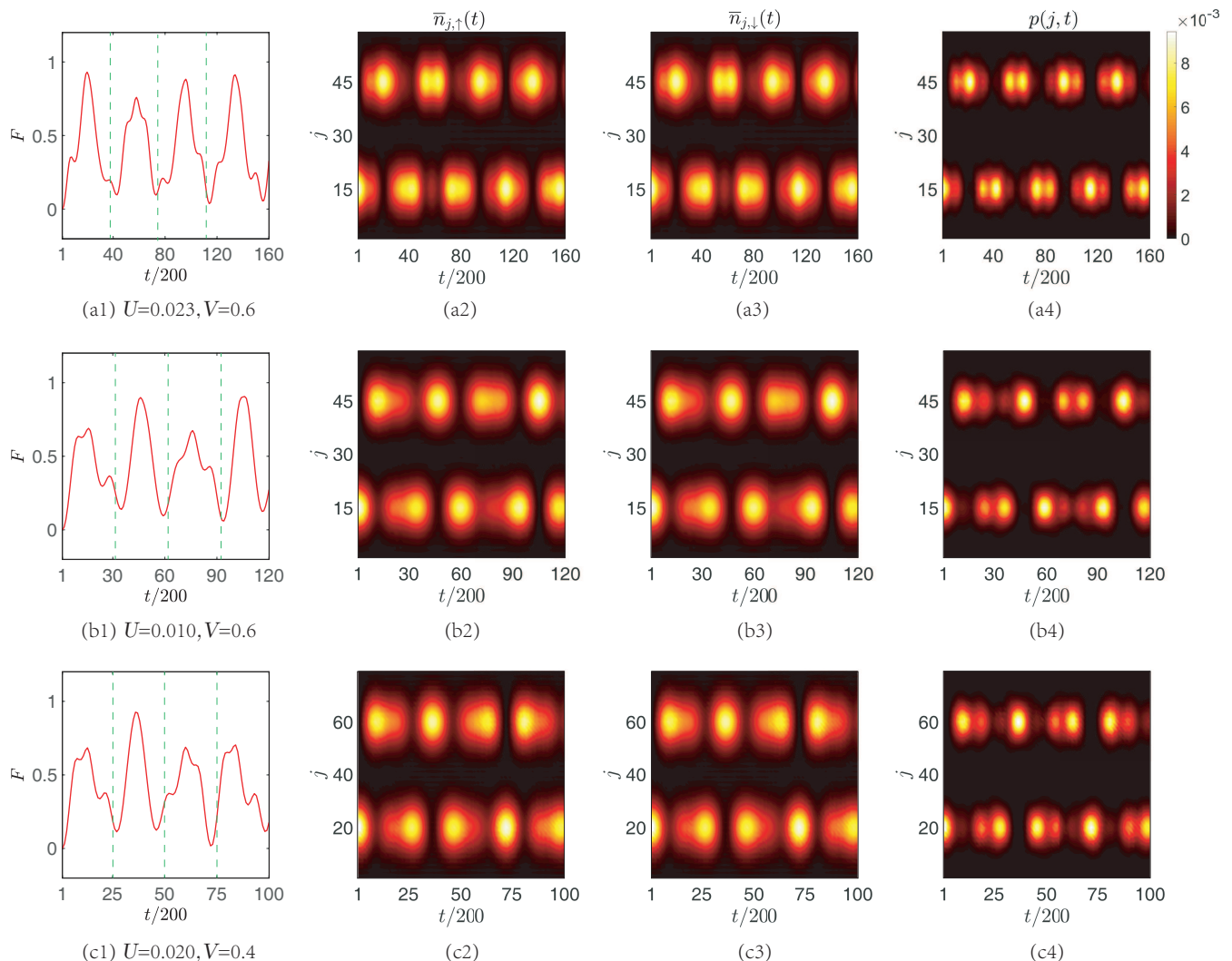


FIG. 6. Numerical results for the dynamical process of pair tunneling, obtained by exact diagonalization. Four quantities, (a1-c1) fidelity (F), (a2-c2) $\bar{n}_{j,\uparrow}(t)$, (a3-c3) $\bar{n}_{j,\downarrow}(t)$, and (a4-c4) $p(j,t)$, defined in Eq. (42) are plotted for the evolved states in systems with four typical parameters. We determine that F , $\bar{n}_{j,\uparrow}$, $\bar{n}_{j,\downarrow}$ and p oscillate approximately with the period indicated by green dotted lines in (a1-c1), obtained from analytical expression $T = 2\pi/\Delta$. Although the fidelity is not perfect, the pair tunneling is evident. The results indicate that the tight-binding approximation works quite well and a bound pair can be near perfectly transferred between two unit cells of superlattice. The system parameters are $n_0 = 30$, $\Delta = 8.3 \times 10^{-4}$, $U = 0.023$, $V = 0.6$ in (a1-a4), $n_0 = 30$, $\Delta = 1.1 \times 10^{-3}$, $U = 0.010$, $V = 0.6$ in (b1-b4), and $n_0 = 40$, $\Delta = 1.3 \times 10^{-3}$, $U = 0.020$, $V = 0.4$ in (c1-c4). The time unit is κ^{-1} and we take $\kappa = 1$.

Taking $\kappa_0 = 0$, $|\psi_I\rangle$ can be set as a initial state for time evolution and $|\psi_I\rangle$ changes to $|\psi_T\rangle$ by sufficient long evolution time. Proper parameters (U and V) are searched to achieve the commensurate energy level structure as in Eq. (37). We plot the schematic illustration of the initial state $|\psi_I\rangle$ and target state $|\psi_T\rangle$ for three typical conditions (see Fig. 5). Obviously, the initial state $|\psi_I\rangle$ and target state $|\psi_T\rangle$ are mutual parity counterpart. The time evolution is computed for $\kappa_0 = 0$ by the formula

$$|\psi(t)\rangle = \exp(-iH_{1M}t)|\psi_I\rangle. \quad (41)$$

We define four quantities

$$\begin{aligned} F(t) &= |\langle \psi_T | \psi(t) \rangle|, \\ \bar{n}_{j,\uparrow}(t) &= \langle \psi(t) | n_{j,\uparrow} | \psi(t) \rangle, \\ \bar{n}_{j,\downarrow}(t) &= \langle \psi(t) | n_{j,\downarrow} | \psi(t) \rangle, \\ p(j,t) &= \langle \psi(t) | n_{j,\uparrow} n_{j,\downarrow} | \psi(t) \rangle, \end{aligned} \quad (42)$$

to clarify our dynamical method. We plot these quantities for three typical conditions in Fig. 6. Numerical results indicate that a pair of electrons can be near perfectly oscillates between two unit cells with different periods. Here the numerical simulation is only performed for the case with $n = 0$, which corresponds to $U_{\text{eff}}/J_{\text{eff}} = 2.309$ from Eq. (36). This ratio is much

larger than $U/\kappa = 0.010 \sim 0.023$ indicated in Fig. 6. Numerical results illustrate that a spatially periodic external field really plays an important role in enhancing the correlation effect. The setting of system parameters is expected to provide guidance for the experiment.

V. SUMMARY

In summary, we demonstrated that the band structure of a simple one-dimensional Hubbard model can be constructed by applying a commensurate external field. Such a moiré Hubbard model has a midgap flat band for zero U . The midgap physics can be well described by an effective Hubbard model when a weak U is switched on. The effective strengths of hopping and Hubbard interaction are controlled by the amplitude and period of the external field. This makes it possible to observe strongly correlated behaviors in a weak correlated system by adding proper spatially periodic external

field. Numerical simulations are performed for the finite-sized moiré Hubbard system to demonstrate the validity of this approach. (i) We demonstrated that there exists a set of bound-pair energy levels, including the η -pairing state. It indicates that the tight-binding approximation works well. (ii) We further presented the phenomenon of bound-pair oscillation, which reveals the dynamics occurring in a moiré Hubbard system with relative strong correlation. The phenomenon of oscillation indicates that the on-site Hubbard interaction in the unit of hopping strength can be enhanced by more than 2 orders. This work provides a method to enhance the correlated effect by the spatially periodic external field and is expected as guidance for the experiment.

ACKNOWLEDGMENTS

This work was supported by National Natural Science Foundation of China (under Grant No. 11874225).

-
- [1] Rafi Bistritzer, and Allan H. MacDonald, Moiré bands in twisted double layer graphene, *Proc. Natl Acad. Sci. USA* **108**, 12233–12237 (2011).
- [2] Y. Cao, J. Y. Luo, V. Fatemi, S. Fang, J. D. Sanchez-Yamagishi, K. Watanabe, T. Taniguchi, E. Kaxiras, and P. Jarillo-Herrero, Superlattice-Induced Insulating States and Valley-Protected Orbits in Twisted Bilayer Graphene. *Phys. Rev. Lett.* **117**, 116804 (2016).
- [3] Yuan Cao, Valla Fatemi, Ahmet Demir, Shiang Fang, Spencer L. Tomarken, Jason Y. Luo, J. D. Sanchez-Yamagishi, K. Watanabe, T. Taniguchi, E. Kaxiras, R. C. Ashoori, and P. Jarillo-Herrero, Correlated insulator behaviour at half-filling in magic-angle graphene superlattices, *Nature* **556**, 80–84 (2018).
- [4] Yuan Cao, Valla Fatemi, Shiang Fang, Kenji Watanabe, Takashi Taniguchi, Efthimios Kaxiras, and Pablo Jarillo-Herrero, Unconventional superconductivity in magic-angle graphene superlattices, *Nature* **556**, 43–50 (2018).
- [5] Kyoungwan Kim, Ashley DaSilva, Shengqiang Huang, Babak Fallahazad, Stefano Larentis, Takashi Taniguchi, Kenji Watanabe, Brian J. LeRoy, Allan H. MacDonald, and Emanuel Tutuc, Tunable moiré bands and strong correlations in small twist angle bilayer graphene. *Proc. Natl Acad. Sci. USA* **114**, 3364–3369 (2017).
- [6] Matthew Yankowitz, Shaowen Chen, Hryhorii Polshyn, Yuxuan Zhang, K. Watanabe, T. Taniguchi, David Graf, Andrea F. Young, and Cory R. Dean, Tuning superconductivity in twisted bilayer graphene, *Science* **363**, 1059–1064 (2019).
- [7] Xiaobo Lu, Petr Stepanov, Wei Yang, Ming Xie, Mohammed Ali Aamir, Ipsita Das, Carles Urgell, Kenji Watanabe, Takashi Taniguchi, Guangyu Zhang, Adrian Bachtold, Allan H. MacDonald, and Dmitri K. Efetov, Superconductors, orbital magnets and correlated states in magic-angle bilayer graphene. *Nature* **574**, 653–657 (2019).
- [8] M. Yankowitz, J. Xue, D. Cormode, J. D. Sanchez-Yamagishi, K. Watanabe, T. Taniguchi, P. Jarillo-Herrero, P. Jacquod, and B. J. LeRoy, Emergence of superlattice Dirac points in graphene on hexagonal boron nitride, *Nat. Phys.* **8**, 382–386 (2012).
- [9] L. A. Ponomarenko, R. V. Gorbachev, G. L. Yu, D. C. Elias, R. Jalil, A. A. Patel, A. Mishchenko, A. S. Mayorov, C. R. Woods, J. R. Wallbank, M. Mucha-Kruczynski, B. A. Piot, M. Potemski, I. V. Grigorieva, K. S. Novoselov, F. Guinea, V. I. Fal’ko, and A. K. Geim, Cloning of Dirac fermions in graphene superlattices, *Nature (London)* **497**, 594–597 (2013).
- [10] C. R. Dean, L. Wang, P. Maher, C. Forsythe, F. Ghahari, Y. Gao, J. Katoch, M. Ishigami, P. Moon, M. Koshino, T. Taniguchi, K. Watanabe, K. L. Shephard, J. Hone, and P. Kim, Hofstadter’s butterfly and the fractal quantum Hall effect in moiré superlattices, *Nature (London)* **497**, 598–602 (2013).
- [11] B. Hunt, J. Sanchez-Yamagishi, A. Young, M. Yankowitz, B. J. LeRoy, K. Watanabe, T. Taniguchi, P. Moon, M. Koshino, P. Jarillo-Herrero, and R. C. Ashoori, Massive Dirac Fermions and Hofstadter Butterfly in a van der Waals Heterostructure, *Science* **340**, 1427–1430 (2013).
- [12] C. R. Woods, L. Britnell, A. Eckmann, R. S. Ma, J. C. Lu, H. M. Guo, X. Lin, G. L. Yu, Y. Cao, R. V. Gorbachev, A. V. Kretinin, J. Park, L. A. Ponomarenko, M. I. Katsnelson, Yu. N. Gornostyrev, K. Watanabe, T. Taniguchi, C. Casiraghi, H-J. Gao, A. K. Geim, and K. S. Novoselov, Commensurate–incommensurate transition in graphene on hexagonal boron nitride, *Nat. Phys.* **10**, 451–456 (2014).
- [13] Shuta Nakajima, Takafumi Tomita, Shintaro Taie, Tomohiro Ichinose, Hideki Ozawa, Lei Wang, Matthias Troyer, and Yoshiro Takahashi, Topological Thouless pumping of ultracold fermions, *Nat. Phys.* **12**, 296–300 (2016).
- [14] M. Lohse, C. Schweizer, O. Zilberberg, M. Aidelsburger, and I. Bloch, A Thouless quantum pump with ultracold bosonic atoms in an optical superlattice, *Nat. Phys.* **12**, 350–354 (2016).

- [15] R. Wang, P. Wang, K. L. Zhang, and Z. Song, Moiré pattern of a spin liquid and a Néel magnet in the Kitaev model, *Phys. Rev. B* **102**, 094207 (2020).
- [16] R. Wang, X. M. Yang, Z. Song, Localization transitions and mobility edges in quasiperiodic ladder, arXiv:1912.04506.
- [17] X. M. Yang, X. Z. Zhang, C. Li and Z. Song, Dynamical signature of the moiré pattern in a non-Hermitian ladder, *Phys. Rev. B* **98**, 085306 (2018).
- [18] Hal Tasaki, The Hubbard model - an introduction and selected rigorous results, *J. Phys. C* **10**, 4353 (1998).
- [19] Fabian H. L. Essler, Holger Frahm, Frank Gohmann, Andreas Klumper, and Vladimir E. Korepin, *The One-Dimensional Hubbard Model*, Cambridge University Press, Cambridge (2005).
- [20] L. Jin, B. Chen, and Z. Song, Coherent shift of localized bound pairs in the Bose-Hubbard model, *Phys. Rev. A* **79**, 032108 (2009).
- [21] L. Jin, and Z. Song, Perfect coherent shift of bound pairs in strongly correlated systems, *Phys. Rev. A* **83**, 052102 (2011).
- [22] Chen Ning Yang, η Pairing and Off-Diagonal Long-Range Order in a Hubbard Model, *Phys. Rev. Lett.* **63**, 2144 (1989).
- [23] Giacomo Corrielli, Andrea Crespi, Giuseppe Della Valle, Stefano Longhi, and Roberto Osellame, Fractional Bloch Oscillations in photonic lattices, *Nat. Commun.* **4** 1555 (2013).